

We are IntechOpen, the world's leading publisher of Open Access books Built by scientists, for scientists

6,900

Open access books available

185,000

International authors and editors

200M

Downloads

Our authors are among the

154

Countries delivered to

TOP 1%

most cited scientists

12.2%

Contributors from top 500 universities



WEB OF SCIENCE™

Selection of our books indexed in the Book Citation Index
in Web of Science™ Core Collection (BKCI)

Interested in publishing with us?
Contact book.department@intechopen.com

Numbers displayed above are based on latest data collected.
For more information visit www.intechopen.com



ASCCC Fractal and Its Application in Antenna Miniaturization

Zeinab Eskandari, Asghar Keshtkar,
Javad Ahmadi-Shokouh and Leila Ghanbari

Additional information is available at the end of the chapter

<http://dx.doi.org/10.5772/intechopen.68431>

Abstract

In this chapter, ASCCC fractal is defined. The name “ASCCC” is based on the process that the fractal is built. It is made by adding and subtracting circles to the circumference of a circle. Then the necessary formulas to build up the first and higher orders of ASCCC fractal are derived. By calculating the perimeter of each order, it is shown that the ASCCC fractal has a great capability in antenna miniaturization. Based on first-order ASCCC fractal, a systematic approach is designed to miniaturize an antipodal dipole at any arbitrary frequency. Then the proposed method is applied at band LTE13 (746–787 MHz), which is controversy for mobile antenna, because it causes the size of a common antenna to become very large for a handheld mobile. It is illustrated that not only the ASCCC fractal is successful in miniaturization of dipole antenna, but also it is very good at improving the antenna’s efficiency in comparison with its counterparts like Koch dipole/monopole.

Keywords: fractal antenna, antenna miniaturization, antenna’s efficiency, antipodal dipole antenna, mobile antenna

1. Introduction

Nowadays, there is demand for antennas which fit in small space while have good radiation performance. Therefore, miniaturization techniques are inevitable in antenna design. Most of miniaturization techniques are based on slot loading, lumped loading, material loading, meandering, using fractal shapes or meta-materials. Generally, these techniques cause radiation efficiency and bandwidth to reduce. The antenna performance can be improved if the available volume within the Chu’s sphere is used effectively. Fractal, meander and volumetric antennas are based on this method [1]. However, volumetric antennas are not suitable for

planar structures. The meander antennas [2] and some fractal antennas such as Hilbert [1] and Koch dipole/monopole [3, 4] have some sections of cancelling current from adjacent conductors that cause the efficiency not to improve significantly. Furthermore, the resonance frequency cannot be found analytically because the physical length is not equivalent with electrical length [1, 2].

In this chapter, a novel fractal named adding and subtracting circles to the circumference of a circle (ASCCC) is defined and the required formulas are derived to build it. The ASCCC fractal is made by adding and subtracting an even number of circles on circumference of a circle, in brief named as adding and subtracting circles to the circumference of a circle (ASCCC). Then, a procedure is shown to miniaturize an antipodal dipole based on first order of ASCCC fractal at any arbitrary frequency. A formula is extracted to determine the resonance frequency of the ASCCC dipole with excellent precision. The proposed procedure is used to design a mobile antenna at challenging band of LTE13 (746–787 MHz). Because of low frequency nature of LTE13, the in-building penetration and area coverage are very good [6]. On the other hand, the size of antenna becomes so large at LTE13 that it is not suitable for a handheld mobile [7]. Therefore, some miniaturization techniques should be applied to the design. One of the great advantages of ASCCC dipole antenna is using the Chu's sphere so effectively that the antenna's efficiency improves considerably in addition to antenna miniaturization. Actually, the currents in adjacent teeth of ASCCC fractal dipole do not weaken the effect of each other, so very good efficiency is obtained. This advantage also makes the physical length to be approximately equal with electrical length.

The design is simulated by full-wave software (Ansoft-HFSS version 15). The results of simulation and measurement are in very good agreement. The efficiency of the proposed dipole antenna is higher than the existing works at LTE13 for handheld mobile antenna [8–25]. Also, the design obtains 40% size reduction compared with a common dipole. Furthermore, the ASCCC design has advantages of being planar and vialess [5].

In Section 2, the ASCCC fractal is explained. Then in Section 3, a procedure is shown to use ASCCC fractal in arms of an antipodal dipole. Theoretically, how to design an ASCCC dipole antenna for a special band is discussed. Next, a mobile antenna is designed, simulated and measured at LTE13. Finally, the conclusion is presented in Section 4.

2. ASCCC fractal

ASCCC fractal is based on adding and subtracting an even number of circles alternately on circumference of an initial circle. In brief, it is named as adding and subtracting circles to the circumference of a circle (ASCCC). It should be noted that radius of secondary circles (R_2) must be smaller than the radius of initial circles (R_1). To make ASCCC fractal clear, firstly consider a circle with radius R_1 as shown in **Figure 1(a)**. Then, arbitrary even numbers of circles (n_1) with radius R_2 ($R_2 < R_1$) are placed to the circumference of **Figure 1(a)** such that their centres are on the initial circle and two adjacent circles have two common points that one of them is on the circumference of initial circle and the other one is inside of it. These conditions lead n_1 to be at least 4 (for $n_1 = 2$, two adjacent circles have two common points but both of them are on the circumference of initial circle and $R_2 > R_1$) and secondary circles cover whole circumference of

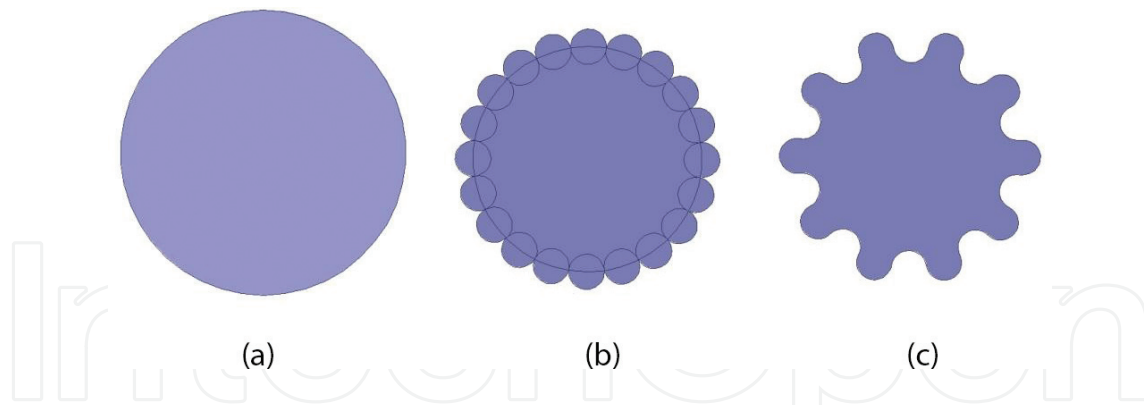


Figure 1. ASCCC fractal with $R_1 = 21$ mm and $n_1 = 20$ (a) initial circle, (b) 20 secondary circles with $R_2 = 3.295$ mm are placed on the circumference of initial circle and (c) secondary circles are united and subtracted alternately [5].

the initial circle. For example, **Figure 1(b)** shows 20 secondary circles that have been placed on an initial circle with $R_1 = 21$ m. **Figure 1(c)** illustrates how secondary circles are added and subtracted alternately. The radius of the secondary circles (R_2) is calculated as follows. Firstly, it is supposed that each secondary circle occupies 2θ angle on the initial circle as in **Figure 2(a)**. Two radiuses of R_1 and one radius of R_2 can make an isosceles triangle with a θ vertex angle as in **Figure 2(b)**. Then, its two leg length and base length are equal to R_1 and R_2 , respectively. R_2 is determined by a trigonometric relationship as in Eq. (1) with respect to **Figure 2(c)**. It should be noted that the value of θ is known because 2θ is related to n_1 as in Eq. (2). If Eq. (2) is substituted in Eq. (1) and some simplifications are done, the R_2 can be written as in Eq. (3).

$$\sin \frac{\theta}{2} = \frac{R_2}{2R_1} \rightarrow R_2 = 2R_1 \sin \frac{\theta}{2} \quad (1)$$

$$2\theta = \frac{2\pi}{n_1} \rightarrow \theta = \frac{\pi}{n_1} \quad (2)$$

$$R_2 = 2R_1 \sin (\pi/2n_1) \quad (3)$$

Zero, first and second orders of ASCCC fractal for $R_1 = 21$ mm, $n_1 = 12$ and $n_2 = 10$ are shown in **Figure 3(a)–(c)**. **Figure 4(a)–(c)** illustrates the stages of producing **Figure 3(a)–(c)**.

Perimeter of the first-order ASCCC (P_1) is equal to perimeter of $n_1/2$ full circle with radius R_2 . So, it is determined by Eq. (4). To understand clearly Eq. (4), firstly consider two adjacent circles shown in **Figure 1(b)**. One of them is supposed to be added (united) and another one is subtracted from the initial circle. Therefore, the effect of these two adjacent circles on the perimeter of **Figure 1(c)** is equal to the circumference of one full circle with radius R_2 . Since the total number of secondary circles is n_1 , the total perimeter of **Figure 1(c)** is equal to $(n_1/2)(2\pi R_2)$.

$$P_1 = (n_1/2)(2\pi R_2) \quad (4)$$

For calculating the perimeter of the second-order ASCCC fractal (P_2), as it is made of $(n_1/2)$ full-circle that each has $n_2/2$ full-circles with radius R_3 ; therefore, its perimeter is equal to the perimeter of a total number of $(n_1/2)(n_2/2)$ full-circle with radius R_3 as in Eq. (5).

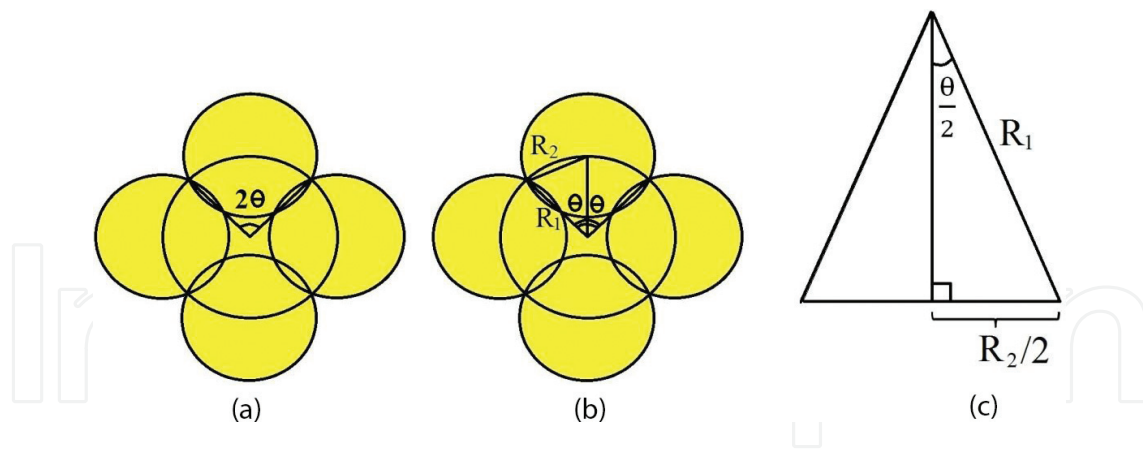


Figure 2. (a) A secondary circle occupies 2θ angle on the initial circle, (b) the radiuses of initial circle and secondary circle make an isosceles triangle with a θ vertex angle and (c) R_1 and R_2 in the isosceles triangle.

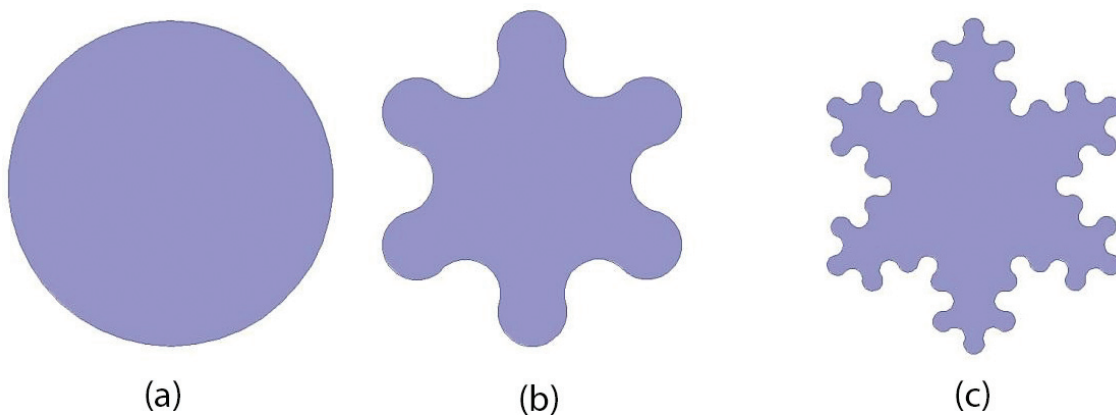


Figure 3. ASCCC fractal for $R_1 = 21$ mm, $n_1 = 12$ and $n_2 = 10$ (a) initial circle with $R_1 = 21$ mm, (b) first-order ASCCC with $n_1 = 12$ and (c) second-order ASCCC with $n_2 = 10$ [5].

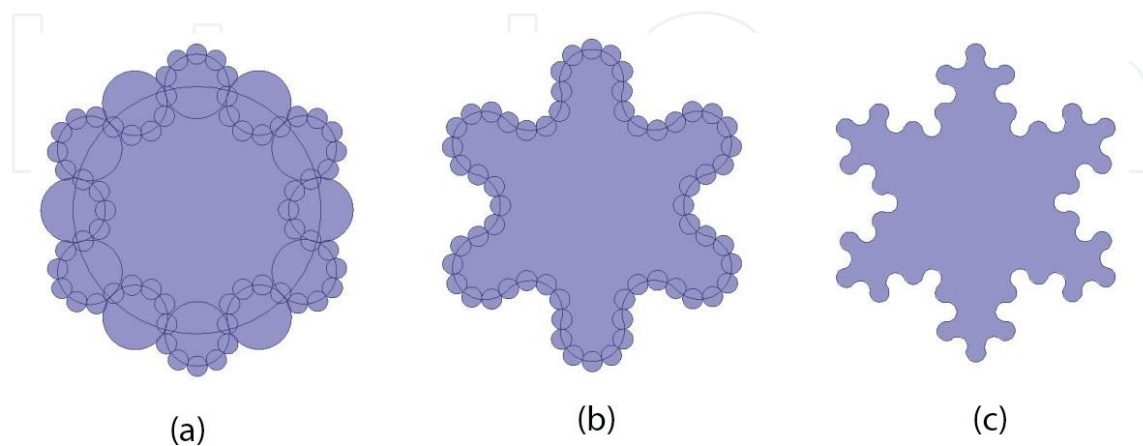


Figure 4. An illustration for building of second-order ASCCC fractal (a) for simplicity, third-order circles are placed only on inner (outer) edge of secondary circles which are supposed to be subtracted (added). (b) Secondary circles are added and subtracted alternately and (c) third circles are added and subtracted alternately [5].

$$P_2 = (n_1/2)(n_2/2)(2\pi R_3) = (n_1/2)(n_2/2) \left(2\pi \times 4R_1 \sin(\pi/2n_1) \sin(\pi/2n_2) \right) \quad (5)$$

Eqs. (6) and (7) show the ratio of P_1 and P_2 to the perimeter of initial circle (P_0), respectively. If n_1 and n_2 have large values, sine function could be approximated by its argument. Then, Eqs. (6) and (7) can be written as $(\pi/2)$ and $(\pi/2)^2$, respectively. Therefore, the perimeter of ASCCC fractal can be multiplied by $(\pi/2)$ in each order.

$$\frac{P_1}{P_0} = \frac{2n_1\pi R_1 \sin(\pi/2n_1)}{2\pi R_1} = n_1 \sin(\pi/2n_1) \quad (6)$$

$$\frac{P_2}{P_0} = \frac{2n_1n_2\pi R_1 \sin(\pi/2n_1) \sin(\pi/2n_2)}{2\pi R_1} = n_1n_2 \sin(\pi/2n_1) \sin(\pi/2n_2) \quad (7)$$

Now, it is time to compare P_1 (the perimeter of the first-order ASCCC with initial (R_1) and secondary (R_2) radiuses) to the circumference C_1 of a common circle with radius $R_1 + R_2$ that occupies the same space on a board. Eq. (8) shows the ratio of P_1 to C_1 . Eq. (9) presents the solutions of Eq. (8) for different n_1 . When the argument of sine is much smaller than unity, the sine can be approximated to its argument. Therefore, approximation $\sin(\pi/2n_1) \approx \pi/2n_1$ is used for $n_1 \geq 10$. As it is seen, the ratio [Eq. (9)] is greater than one for $n_1 \geq 6$, so P_1 is larger than C_1 . Therefore, if a way is found to force the current to travel the perimeter P_1 , antenna miniaturization is obtained for $n_1 \geq 6$ [5].

$$\frac{P_1}{C_1} = \frac{2n_1\pi R_1 \sin(\pi/2n_1)}{2\pi(R_1 + R_2)} = \frac{n_1 \sin(\pi/2n_1)}{1 + 2 \sin(\pi/2n_1)} \quad (8)$$

$$\frac{P_1}{C_1} = \begin{cases} 0.867 & n_1 = 4 \\ 1.023 & n_1 = 6 \\ 1.122 & n_1 = 8 \\ 1.191 \leq \frac{\pi/2}{1 + (\pi/n_1)} \leq \frac{\pi}{2} & n_1 \geq 10 \end{cases} \quad (9)$$

3. An application of ASCCC fractal in antenna miniaturization

In this section, it is shown that an antipodal dipole antenna is miniaturized by applying the first-order ASCCC fractal to arms of the dipole antenna. The procedure could be applied to any arbitrary frequency [5].

3.1. The proposed design

In this section, it is shown that an antipodal dipole antenna is miniaturized by applying the first-order ASCCC fractal to arms of the dipole antenna. **Figure 5(a)–(d)** presents the utilized method. In the first step, two first-order ASCCC fractals with the same n_1 but different R_1 are designed (**Figure 5(a)**). To distinguish R_1 of fractals, R_{1i} is chosen for inner fractal and R_{1o} for outer fractal. In the next step, the inner fractal is subtracted from the outer fractal as shown in **Figure 5(b)**. Then, the shape is split into two equal halves as shown in **Figure 5(c)**. Finally, each

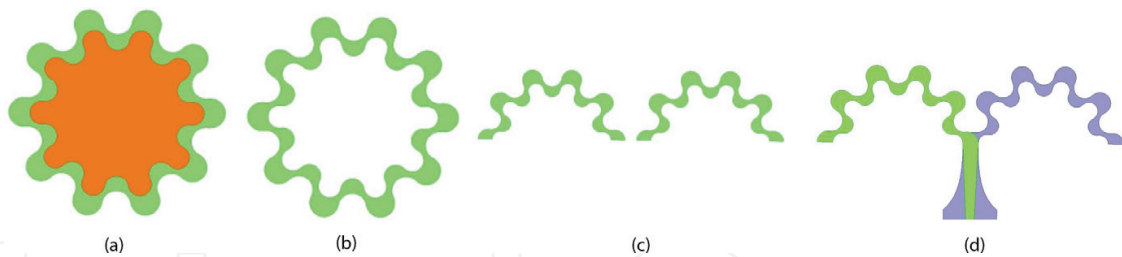


Figure 5. A method to use ASCCC fractal in arms of an antipodal dipole antenna (a) two first-order ASCCC fractal with same n_1 but different R_1 are designed, (b) inner fractal is subtracted from the outer one, (c) the shape is split into two equal halves and (d) each half is employed as an arm in an antipodal dipole antenna [5].

half is employed as an arm in a balanced antipodal dipole as illustrated in **Figure 5(d)**. The first resonance of the proposed dipole is calculated by Eq. (10). In Eq. (10), c is the speed of light and λ is the resonance wavelength.

$$f = c/\lambda \quad (10)$$

In a common dipole antenna, the length in which current travels along the two arms is equal to $\lambda/2$ of the first resonance wavelength. In calculation of $\lambda/2$, it should be noted that current tends to travel the shortest path. In **Figure 5(d)**, the current is confined to area between inner and outer fractals. The perimeter of inner fractal is shorter than the perimeter of outer one. Therefore, the inner fractal perimeter is more likely to be tracked. To be sure that current does not find any shorter path than the inner perimeter, R_{1o} should be chosen as close to R_{1i} as possible. As a result, the current travelling length is approximately equal to the inner fractal perimeter that is determined by using Eq. (4). Then, the resonance frequency could be written as in Eq. (11). In Eq. (11), P_{1i} is the perimeter of inner fractal in **Figure 5(d)**.

$$f = \frac{c}{\lambda} = \frac{c}{2P_{1i}} = \frac{c}{4n_1\pi R_{1i} \sin(\pi/2n_1)} \quad (11)$$

To design a balanced feedline, the method described in Refs. [26] and [27] is used. The line parameters are given in **Figure 6**. The exponential part of line is made by Eqs. (12) and (13). W_{cps} is equal to $(R_{1o} + R_{2o}) - (R_{1i} + R_{2i})$. L_{exp} , L_{mv} , W_{gnd} and p are arbitrary parameters that are chosen with respect to a good S_{11} result.

$$y = \pm \left[A \times \exp(px) + \left(\frac{W_{cps}}{2} - A \right) \right] \quad (12)$$

$$A = \frac{W_{gnd} - W_{cps}}{2(\exp(p \times L_{exp}) - 1)} \quad (13)$$

3.2. Simulation and measurement results

The method described in Section 3.1 is used to design a handset mobile antenna at the LTE13 band (746–787 MHz). The antenna is printed on an FR4 substrate with $\epsilon_r = 4.4$ and \tan

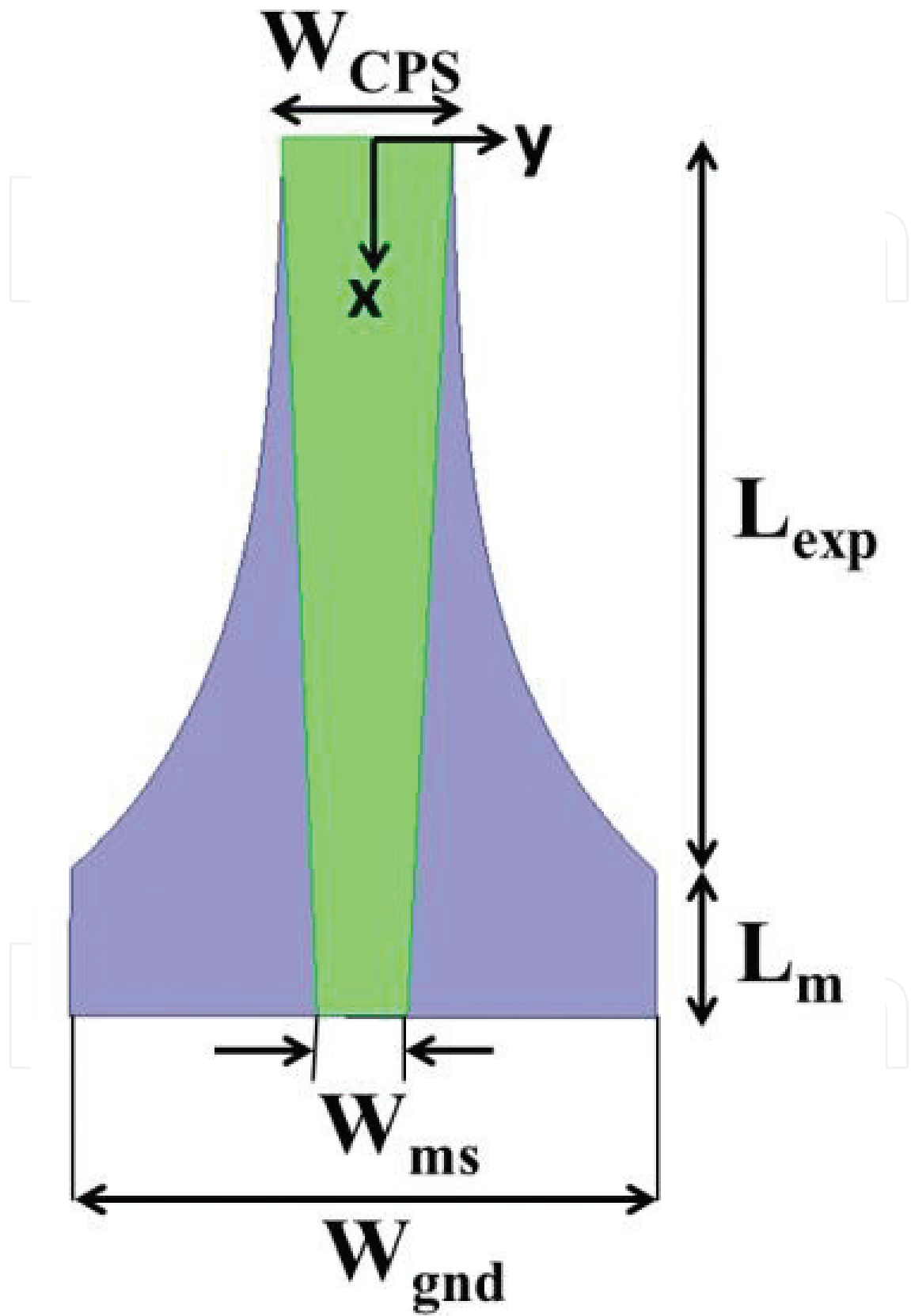


Figure 6. Geometry and parameters of the balanced feedline.

$\delta = 0.02$. Firstly, an initial resonance frequency within band LTE13 should be picked out to determine $\lambda/2$ by Eq. (10). As the length $\lambda/2$ is approximately equal to the perimeter of inner ASCCC, as shown in **Figure 5(a)**, so R_{1i} is determined by Eq. (4). To stay in safe side, a frequency of 750 MHz is picked out for the initial design because a good S_{11} in lower frequencies needs longer length in arms while preparing longer length is harder to obtain. Please note that the value of n_1 is arbitrary. The larger n_1 results in the smaller R_{2i} , so a more compact design is obtained. In the simulations, feedline parameters have been chosen as: $L_m = 5$ mm, $L_{exp} = 25$ mm, $W_{gnd} = 20$ mm, $W_{ms} = 3.04$ mm and $p = 150$.

$R_{1i} = 20.28$ mm is found for $n_1 = 20$ at 750 MHz. To determine a value for R_{1o} , some simulations are done for different R_{1o} radiuses ($R_{1o} = 23, 24.5$ and 26 mm). The simulated S_{11} results are shown in **Figure 7**. As seen, a smaller R_{1o} makes a better confinement of current to the inner fractal perimeter; therefore, the resonance frequency is closer to the initial design. On the other hand, a bigger R_{1o} results in better S_{11} and wider bandwidth because of a larger radiating area. However, $R_{1o} = 23$ mm cannot be chosen. Although resonance frequency is closer to the initial design, the whole band of LTE13 cannot be covered. The problem could be tackled as follows. If a bigger R_{1i} is chosen, the resonance frequency is lowered, so more freedom is prepared to pick out larger values for R_{1o} that could somehow compensate for lowering of frequency while enough bandwidth and good S_{11} are obtained at the LTE13 band. By a little try and error, it is found the whole LTE13 band could be covered with good S_{11} for $R_{1i} = 20.5$ mm and $R_{1o} = 25.5$ mm. As it is seen, the selected R_{1i} is so close to the initial design ($R_{1i} = 20.28$ mm) and the proposed formulas prepare very good primary guess.

A fabricated prototype of the proposed antenna is shown in **Figure 8**. The overall size of the printed antenna is $62 \times 115 \times 1.6$ mm³ that is suitable for a handheld mobile. The simulated and measured results of S_{11} are presented in **Figure 9**. It is seen that there is very good agreement between them. The small resonance at 1.045 GHz is due to the type of feedline.

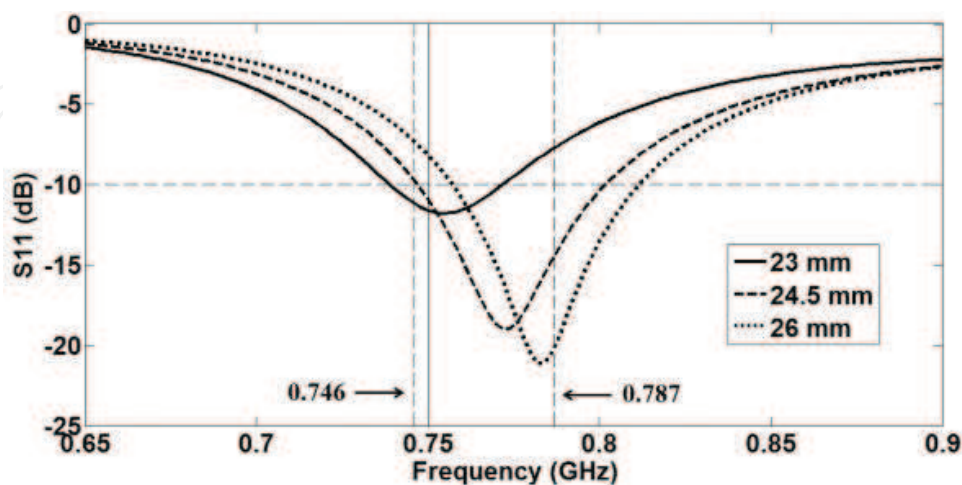


Figure 7. S_{11} parameter for different R_{1o} ($R_{1i} = 20.28$ mm, $n_1 = 20$) [5].

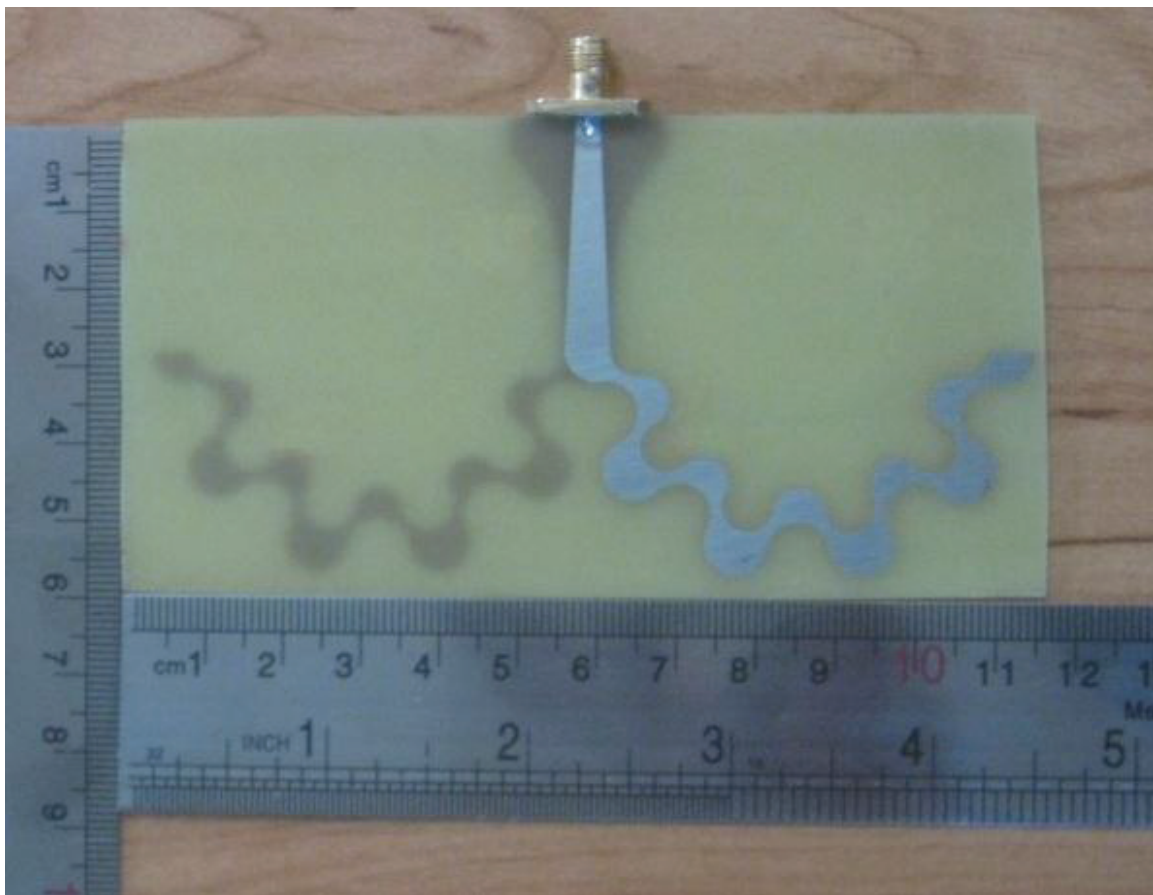


Figure 8. Fabricated prototype of the proposed design [5].

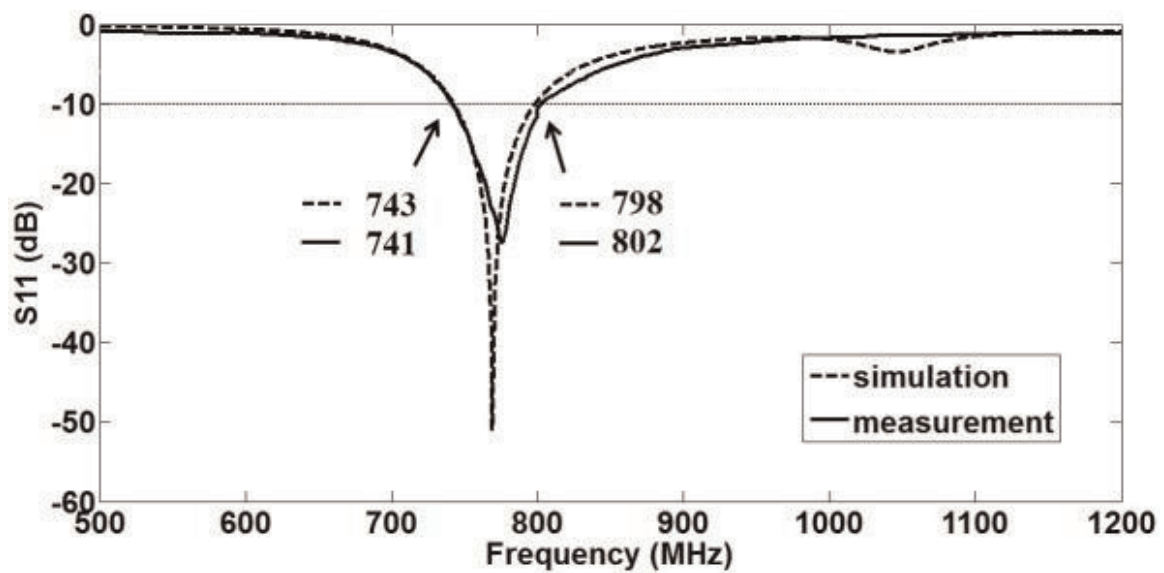


Figure 9. Simulation and measurement results of S_{11} against frequency [5].

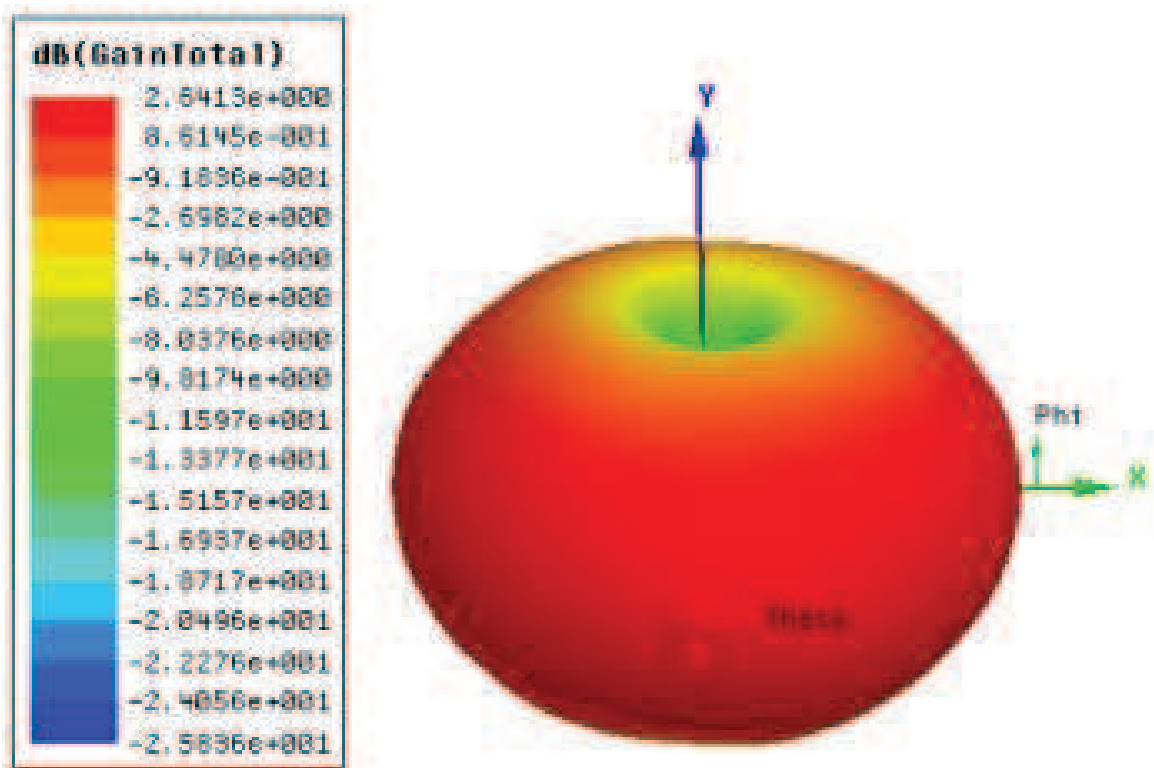


Figure 10. Simulated 3D radiation patterns at 769 MHz [5].

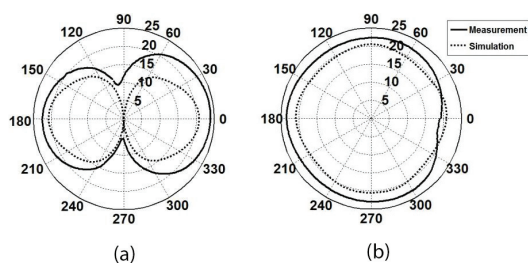


Figure 11. Simulated and measured radiation patterns at 769 MHz (a) E-plane and (b) H-plane [5].

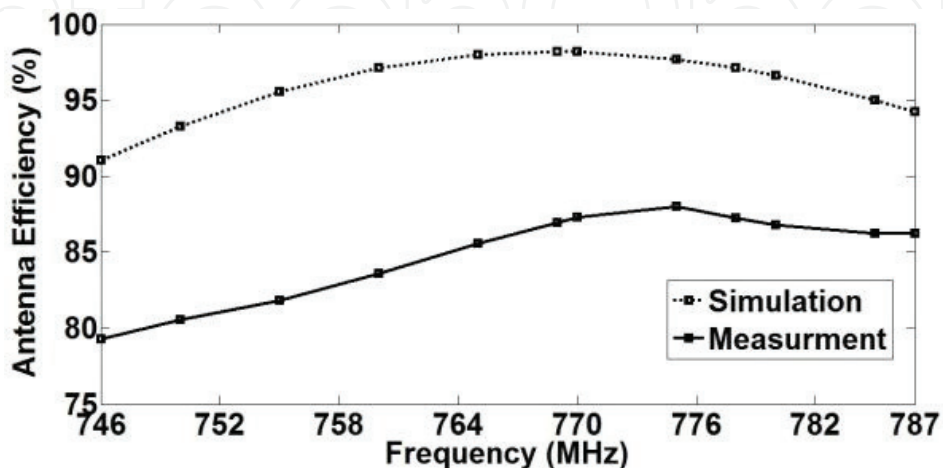


Figure 12. Simulated and measured radiation efficiency for LTE13 [5].

Refs.	[8]	[9]	[10]	[11]	[12]	[13]	[14]	[15]	[16]
Antenna efficiency (%)	45 at 762 MHz	40–60	40–60*	40–51.24	30–55*	34 at 746 MHz	45–55	56–84	52–72
Refs.	[17]	[18]	[19]	[20]	[21]	[22]	[23]	[24]	[25]
Antenna efficiency	50–65	Average 62.85	50–70	53–76	52–75*	40–53*	53–76	45.24–48.43	10–40*

Note: * means the radiation efficiency has been reported in the reference.

Table 1. Antenna efficiency at LTE 13 in different papers.

Figures 10 and **11** present the 3-D and polar radiation patterns of the proposed antenna at 769 MHz, respectively. As they show, the antenna has a dipolar radiation pattern. **Figure 12** shows the efficiency of antenna. The measured efficiency is obtained by the improved Wheeler-cap method [28]. Antenna efficiency varies from 79.28 to 88.01%. As it is seen, the antenna has very high efficiency at LTE13, on the contrary of the other designs for this band that are listed in **Table 1** [8–25].

Finally, the antenna exhibits 40% size reduction in comparison with a common dipole. This is evidence that the proposed procedure is a good technique in antenna miniaturization [5].

4. Conclusion

In this chapter, ASCCC fractal is defined and its driving formulas are extracted. It is shown that ASCCC fractal has a great potential in antenna miniaturization and improving efficiency. A miniaturization method was designed for a dipole antenna at any arbitrary frequency. Then, the method applied to the dipole antenna at band LTE13 which is very challenging for reduction in size of mobile antennas. The total size of antenna is $62 \times 115 \times 1.6 \text{ mm}^3$, which is appropriate for handheld mobiles. The efficiency of antenna is greater than 79% with S_{11} better than -10 dB . The amount of efficiency is considerably higher than existing works.

Author details

Zeinab Eskandari^{1*}, Asghar Keshtkar¹, Javad Ahmadi-Shokouh² and Leila Ghanbari¹

*Address all correspondence to: zeinab.eskandari@hotmail.com

1 Imam Khomeini International University, Qazvin, Iran

2 University of Sistan and Baluchestan, Zahedan, Iran

References

- [1] Volakis J, Chen CC, Fujimoto K. *Small Antennas: Miniaturization Techniques & Applications*. 1st ed. New York: McGraw-Hill; 2010. p. 428

- [2] Hansen RC, Collin RE. *Small Antenna Handbook*. 1st ed. Hoboken, New Jersey: John Wiley & Sons, Inc.; 2011. p. 346
- [3] Best SR. On the performance properties of the koch fractal and other bent wire monopoles. *IEEE Transactions on Antennas and Propagation*. 2003;**51**(6):1292–1300. DOI: 10.1109/TAP.2003.812257
- [4] Vinoy KJ, Abraham JK, Varadan VK. On the relationship between fractal dimension and the performance of multi-resonant dipole antennas using Koch curves. *IEEE Transactions on Antennas and Propagation*. 2003;**51**(9):2296–2303. DOI: 10.1109/TAP.2003.816352
- [5] Eskandari Z, Keshtkar A, Ahmadi-Shokoh J, Ghanbari L. A novel fractal for improving efficiency and its application in LTE mobile antennas. *Microwave and Optical Technology Letters*. 2015;**57**(10):2429–2434. DOI: 10.1002/mop.29346
- [6] Sharawi MS, Numan AB, Khan MU, Aloji DN. A dual-element dual-band MIMO antenna system with enhanced isolation for mobile terminals. *IEEE Antennas and Wireless Propagation Letters*. 2012;**11**:1006–1009. DOI: 10.1109/LAWP.2012.2214433
- [7] Zhang Z. *Antenna Design for Mobile Devices*. 1st ed. Singapore: John Wiley & Sons (Asia) Pte Ltd; 2011. p. 280
- [8] Meshram MK, Animeh RK, Pimpale AT, Nikolova N K. A novel quad-band diversity antenna for LTE and Wi-Fi applications with high isolation. *IEEE Transactions on Antennas and Propagation*. 2012;**60**(9):4360–4371. DOI: 10.1109/TAP.2012.2207044
- [9] Yu Y, Kim G, Ji J, Seong W. A compact hybrid internal MIMO antenna for LTE application. In: *2010 Proceedings of the Fourth European Conference on Antennas and Propagation (EuCAP)*; 12–16 April 2010; Barcelona, Spain: IEEE; 2010.
- [10] Lopez N, Lee C-J, Gummalla A, Achour M. Compact metamaterial antenna array for long term evolution (LTE) handset application. In: *IEEE International Workshop on Antenna Technology (iWAT) 2009*; 2–4 March 2009; Santa Monica, CA, USA: IEEE; 2009. DOI: 10.1109/IWAT.2009.4906933
- [11] Bae H, Harackiewicz FJ, Park MJ, Kim T, Kim N, Kim D. Compact mobile handset MIMO antenna for LTE700 applications. *Microwave and Optical Technology Letters*. 2010;**52**(11):2419–2422. DOI: 10.1002/mop.25507
- [12] Zhao X, Choi J. Design of a MIMO antenna with low ECC for a 4G mobile terminal. *Microwave and Optical Technology Letters*. 2014;**56**(4):965–970. DOI: 10.1002/mop.28196
- [13] Cheon Y, Lee J, Lee J. Quad-band monopole antenna including LTE 700 MHz with magneto-dielectric material. *IEEE Antennas and Wireless Propagation Letters*. 2012;**11**:137–140. DOI: 10.1109/LAWP.2012.2184517

- [14] Ban YL, Chen JH, Yang S, Li JLW, Wu YJ. Low-profile printed octa-band LTE/WWAN mobile phone antenna using embedded parallel resonant structure. *IEEE Transactions on Antennas and Propagation*. 2013;**61**(7):3889–3894. DOI: 10.1109/TAP.2013.2258879
- [15] Wong KL. 4G/Multiband handheld device ground antennas. In: *Microwave Conference Proceedings (APMC)*; 5–8 November 2013; Asia-Pacific: IEEE; 2013. DOI: 10.1109/APMC.2013.6695215
- [16] Wong KL, Chang YW. Internal WWAN/LTE handset antenna integrated with USB connector. *Microwave and Optical Technology Letters*. 2012;**54**(5):1154–1159. DOI: 10.1002/mop.26788
- [17] Jeon S, Kim H. Mobile terminal antenna using a planar inverted-e feed structure for enhanced impedance bandwidth. *Microwave and Optical Technology Letters*. 2012;**54**(9):2133–2139. DOI: 10.1002/mop.27035
- [18] Jo Y, Park K, Lee J, Kim HH, Kim H. Mobile handset antenna with parallel resonance feed structures for wide impedance bandwidth. In: *Proceedings of the International Symposium on Antennas & Propagation (ISAP)*; 23–25 October 2013; Nanjing, China: IEEE; 2013.
- [19] Lee J, Liu Y, Kim HH, Kim H. PIFA with dual-resonance feed structure for enhancement of impedance bandwidth. *Electronics Letters*. 2013;**49**(15):921–922. DOI: 10.1049/el.2013.1432
- [20] Chu FH, Wong KL. Planar printed strip monopole with a closely-coupled parasitic shorted strip for eight-band LTE/GSM/UMTS mobile phone. *IEEE Transactions on Antennas and Propagation*. 2010;**58**(10):3426–3431. DOI: 10.1109/TAP.2010.2055807
- [21] Wong KL, Chen WY, Wu CY, Li WY. Small-size internal eight-band LTE/WWAN mobile phone antenna with internal distributed LC matching circuit. *Microwave and Optical Technology Letters*. 2010;**52**(10):2244–2250. DOI: 10.1002/mop.25431
- [22] Ban YL, Liu CL, Chen Z, Li JLW, Kang K. Small-size multiresonant octaband antenna for LTE/WWAN smartphone applications. *IEEE Antennas and Wireless Propagation Letters*. 2014;**13**:619–622. DOI: 10.1109/LAWP.2014.2313353
- [23] Lu JH, Guo JL. Small-size octaband monopole antenna in an LTE/WWAN mobile phone. *IEEE Antennas and Wireless Propagation Letters*. 2014;**13**:548–551. DOI: 10.1109/LAWP.2014.2311797
- [24] Luo J, Gong SX, Duan P, Mou C, Long M. Small-size wideband monopole antenna with CRLH-TL for LTE mobile phone. *Progress in Electromagnetics Research C*. 2014;**50**:171–179.
- [25] Takemura N. Tunable inverted-L antenna with split-ring resonator structure for mobile phones. *IEEE Transactions on Antennas and Propagation*. 2013;**61**(4):1891–1897. DOI: 10.1109/TAP.2012.2232894

- [26] Antoniadou MA, Eleftheriades GV. Multiband compact printed dipole antennas using NRI-TL metamaterial loading. *IEEE Transactions on Antennas and Propagation*. 2012;**60**(12):5613–5626. DOI: 10.1109/TAP.2012.2211324
- [27] Bourqui J, Okoniewski M, Fear EC. Balanced antipodal vivaldi antenna with dielectric director for near-field microwave imaging. *IEEE Transactions on Antennas and Propagation*. 2010;**58**(7):2318–2326. DOI: 10.1109/TAP.2010.2048844
- [28] Geissler M, Litschke O, Heberling D, Waldow P, Wolff I. An improved method for measuring the radiation efficiency of mobile devices. In: *Antennas and Propagation Society International Symposium*. IEEE; 22-27 June 2003; Columbus, Ohio, USA: IEEE; 2003. DOI: 10.1109/APS.2003.1220380

IntechOpen